

Biophysical Journal, Volume 115

Supplemental Information

Passive Permeability of Planar Lipid Bilayers to Organic Anions

Andrea Ebert, Christof Hanneschlaeger, Kai-Uwe Goss, and Peter Pohl

Supporting Material - Passive permeability of planar lipid bilayers to organic anions

Andrea Ebert^{*}, Christof Hanneschläger[†], Kai-Uwe Goss^{**‡}, and Peter Pohl[†]

^{*} Analytical Environmental Chemistry, Helmholtz Centre for Environmental Research – UFZ, Leipzig, Germany;

[†] Institute of Biophysics, Johannes Kepler University, Linz, Austria; [‡] Institute of Chemistry, Martin Luther University, Halle, Germany

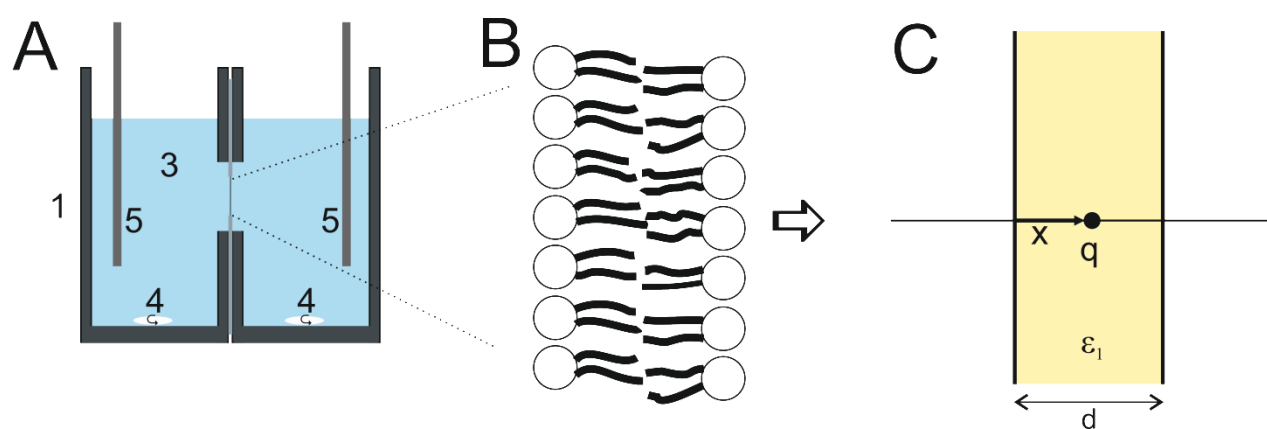


Fig. S1(A) Schematic diagram of the conductance/permeability experiments. The two compartments of a Teflon chamber (1) are separated by a septum (2). Across a thin hole in the septum the planar lipid bilayer is formed. Voltage is applied to electrodes (5) placed in the buffer solutions (3) in both compartments of the Teflon chamber and the resulting current is measured. The buffer solutions are agitated by magnetic stirrers (4). **(B)** Schematic depiction of the planar bilayer consisting of hydrophilic polar head groups and the hydrophobic tails. **(C)** As the main barrier of membrane permeation is assumed to lie in the alkane like center of the membrane, for calculations it is often approximated as a thin slab of hydrophobic medium of width d and permittivity ϵ_1 . This model is also used when calculating the image energy, the electrical interaction between the interfaces and the ion with charge q in the organic phase at distance x from the interface. Drawings are not in scale.

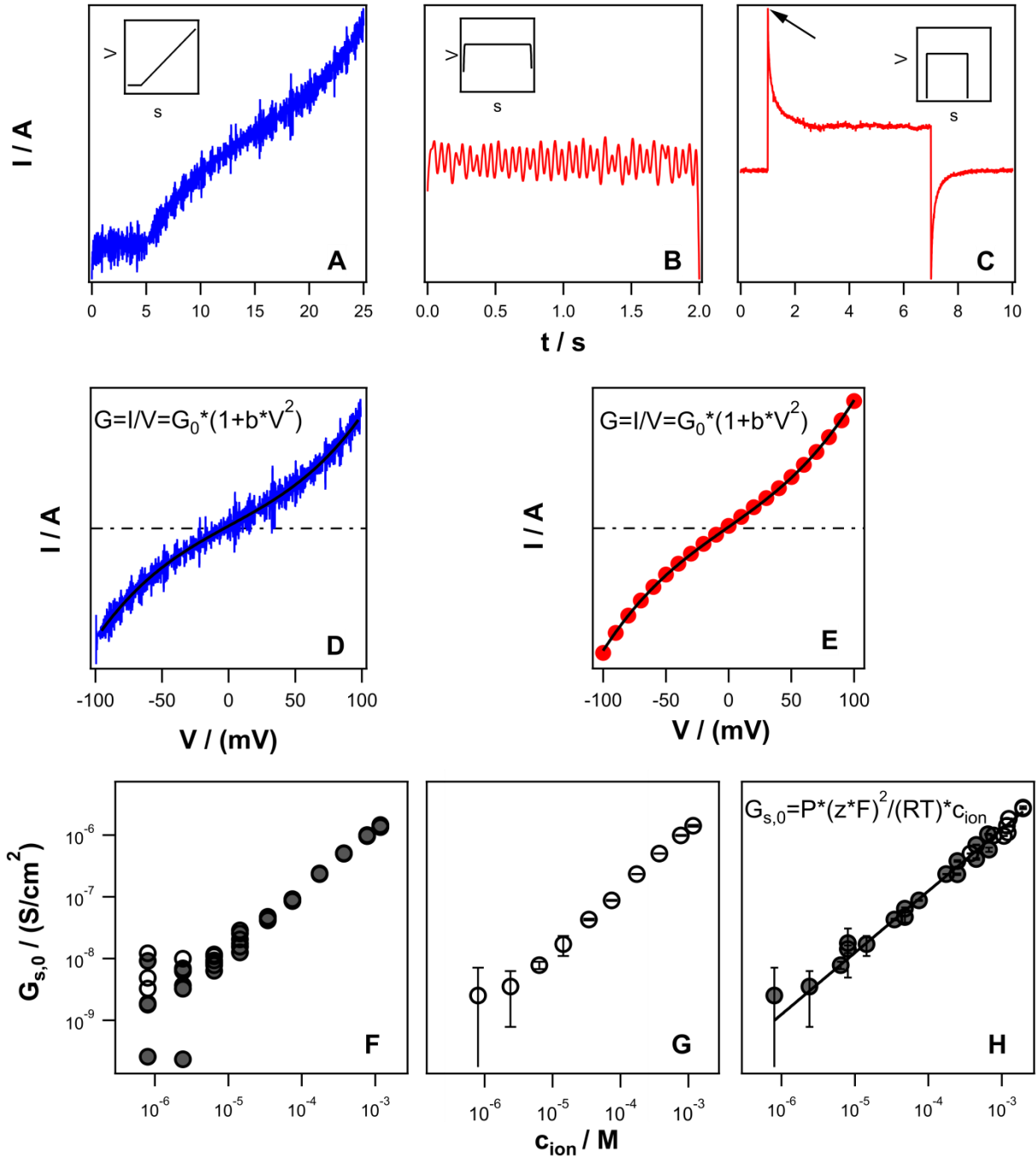


Fig. S2 Electrophysiological measurements and analysis. After each chemical addition, several ramp voltage sweeps (-100mV to +100mV) are recorded (A), and the resulting I/V curves fit by Eq. 9 to extract the conductivity at zero voltage G_0 (D). Due to the built-in on-line compensation of the HEKA EPC10 device the ramps at the rate 10mV/s show no capacitive spikes, and allow a faster measurement than the traditional voltage clamp technique, where different DC-voltages are applied and the steady state current is measured (B). There, a 2s long DC-voltage is increased incrementally by 10mV from -100mV to +100mV, and the resulting I/V curves (E) are likewise fit by Eq. 9. For sporadic control samples, this technique lead to the same G_0 as the ramp sweeps. If the researched chemical's permeation is not limited by the membrane itself, but by diffusion through the unstirred water layers, a voltage step is applied to the membrane to determine the conductance at $t=0s$ just after the voltage is applied (C; arrow marks extracted current value; for the eOne device - without capacitive compensation - the current was extrapolated to zero time, in accordance with Ketterer et al. (1)). The I/V curve is evaluated as before (E). Specific conductivities $G_{0,s}$ for all measured concentrations are gained dividing G_0 by the area of the septum hole, and subtracting the background

conductivity BG that was measured without chemical addition (**F**; filled circles: after BG subtraction; empty circles: before BG subtraction). The mean (open circles) and standard deviation (depicted as error bars) were calculated for all ramp repeats at each concentration within the same experiment (**G**). The permeability was obtained using a linear regression (Eq. 10; Igor Pro) on the combined data of several experiments (**H**). The regression was weighted by the variance of the respective ramp repeats, and DMSO concentrations above 1%v/v were not included in the evaluation (open circles). Calculated standard deviations were not significant, and are therefore not listed in Table 1.

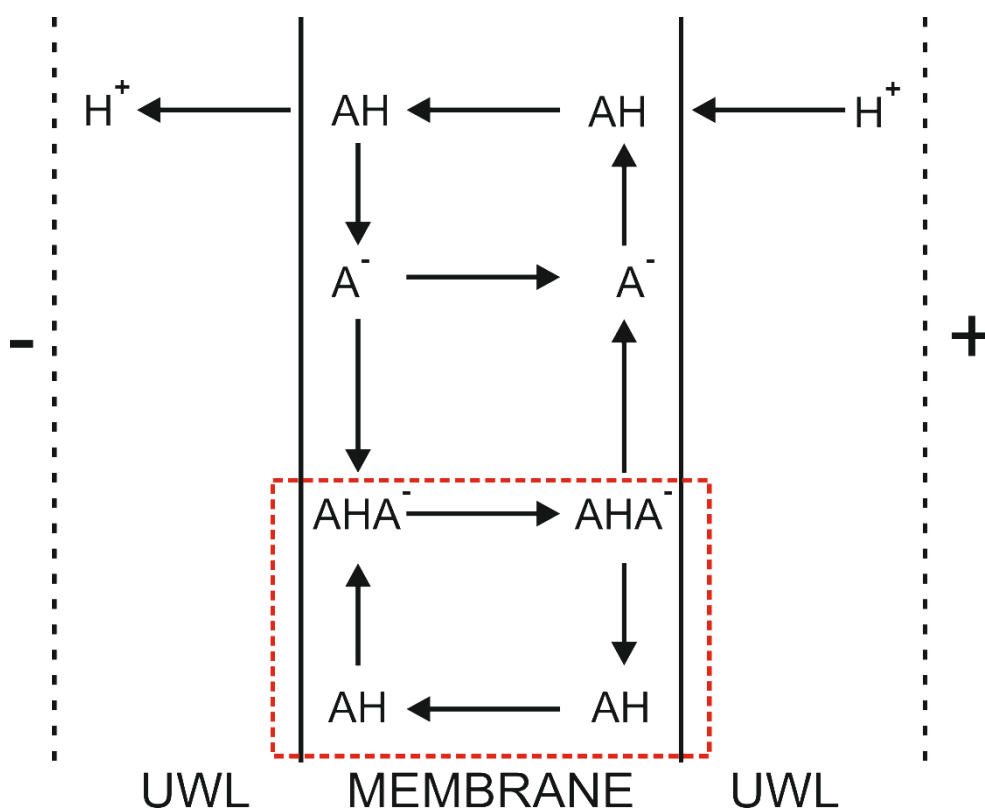


Fig. S3 The process of uncoupling for weak acids: Following the electrical potential, the weak acid traverses the membrane in its charged deprotonated form $[A^-]$. A local concentration gradient builds up, and the protonated form $[AH]$ diffuses back across the membrane, thus carrying an H^+ ion from one side to the other. The monomeric permeability can be measured directly if the limiting process is the permeation of the anion $[A^-]$. But this is not always the case. For one, the parallel permeation of the heterodimer $[AHA^-]$ (red frame), driven by the same gradients, may add to the monomeric permeability or replace it as the limiting permeation process. Secondly, for very fast membrane permeabilities, the diffusion of H^+ through the unstirred water layers UWL may become rate limiting. This can be minimized by the right choice of buffer concentration B, as then the hydrogen flux $j = j_{H^+} + j_{OH^-} + j_{BH}$ may be determined by the diffusion of buffer molecules through the UWL rather than the diffusion of protons (2, 3).

Quadratic heterodimer concentration dependence

In the limit of low heterodimer concentration $[AHA^-]$, the total concentration c_{tot} simplifies to

$$c_{tot} = 2[AHA^-] + [A^-] + [HA] \approx [A^-] + [HA] \quad (S1)$$

Using the Henderson-Hasselbalch equation

$$pH = pK_a + \log([A^-]/[HA]) \quad (S2)$$

the monomer concentrations can be expressed as follows:

$$[A^-] = c_{tot}/(1 + 10^{-pH+pK_a}) \quad (S3)$$

$$[HA] = c_{tot}/(1 + 10^{pH-pK_a}) \quad (S4)$$

The process of dimerization with rate constant K_D may be described as:

$$[A^-] * [HA] * K_D = [AHA^-] \quad (S5)$$

Inserting Eq. S3,4 in Eq. S5 finally leads to the quadratic dependence of heterodimer concentration on c_{tot} :

$$[AHA^-] = c_{tot}^2 * K_D * 1/[(1 + 10^{-pH+pK_a}) * (1 + 10^{pH-pK_a})] \quad (S6)$$

Table S1 Compound Name, Molecular Weight MW, calculated Diffusion Constant D_m inside the membrane^a, Calculated logarithmic Anion-Permeability for an effective bilayer thickness of 25.5Å^b.

| Compound Name | MW | $D_m / (\text{cm}^2/\text{s})$ | Log [$P_{calc} / (\text{cm/s})$] |
|--|-------|--------------------------------|------------------------------------|
| TPB | 319.2 | 5.4×10^{-07} | -1.5 |
| CCCP | 203.6 | 6.7×10^{-07} | -7.2 |
| 6-OH-BDE47 | 500.8 | 4.4×10^{-07} | -7.6 |
| bis(fluorosulfonyl)azanide | 180.1 | 7.1×10^{-07} | -7.7 |
| dino2terb | 239.2 | 6.2×10^{-07} | -8.8 |
| dinoseb | 239.2 | 6.2×10^{-07} | -9.2 |
| PCP | 265.3 | 5.9×10^{-07} | -9.2 |
| bromoxynil | 275.9 | 5.8×10^{-07} | -10.2 |
| triclosan | 288.5 | 5.7×10^{-07} | -10.5 |
| coumachlor | 341.8 | 5.3×10^{-07} | -11.0 |
| 4-nitro-2-(trifluoromethyl)-1H-benzimidazole | 230.1 | 6.3×10^{-07} | -11.0 |
| 3,4-Dnp | 183.1 | 7.0×10^{-07} | -11.5 |
| bromol | 329.8 | 5.4×10^{-07} | -11.7 |

| | | | |
|--------------------------------------|--------|-----------------------|-------|
| 2,4-Dnp | 183.1 | 7.0×10^{-07} | -11.8 |
| warfarin | 307.3 | 5.5×10^{-07} | -12.6 |
| flufenamic acid | 280.2 | 5.8×10^{-07} | -13.8 |
| 3,5-Dcp | 162 | 7.4×10^{-07} | -14.4 |
| 4-Np | 138.1 | 8.0×10^{-07} | -15.1 |
| diclofenac | 295.1 | 5.6×10^{-07} | -16.1 |
| 4-octylbenzenesulfonate | 269.4 | 5.9×10^{-07} | -17.6 |
| sulcotrione | 327.8 | 5.4×10^{-07} | -17.9 |
| salicylic acid | 137.11 | 8.0×10^{-07} | -18.7 |
| 9,10-dimethoxyanthracene-2-sulfonate | 317.3 | 5.5×10^{-07} | -19.3 |
| anthracene-9-carboxylic acid | 221.2 | 6.4×10^{-07} | -20.0 |

^a Diffusion constants inside the membrane at 25°C were predicted from molecular weight using the formula $D_m = 1/10 * D_{aq} = 10^{-5.13 - 0.453 * \log(MW)}$, as explained in detail in Ref. (4) and (5). ^b Image energies were calculated according to Eq. 8 for an effective bilayer thicknesses of 25.5 Å. The predicted bulk hexadecane/water partition coefficients (COSMOtherm) were corrected for both image and dipole energy in the membrane, and the permeability was then calculated using Eq. 2.

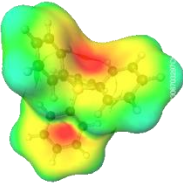
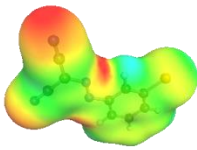
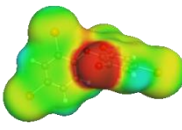
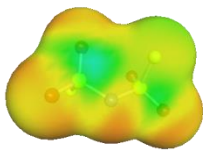
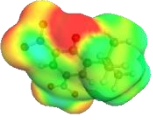
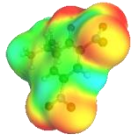
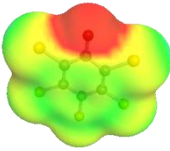
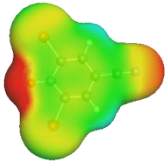
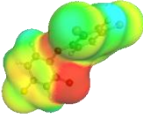
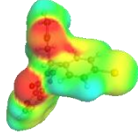
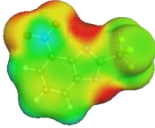
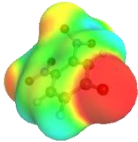
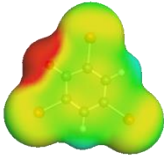
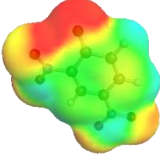
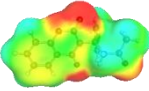
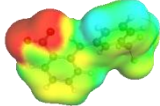
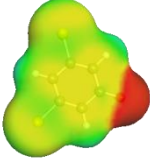
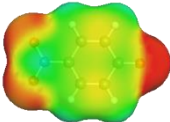
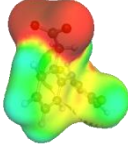
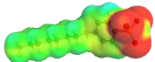
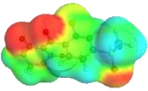
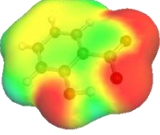
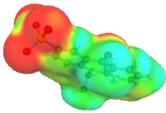
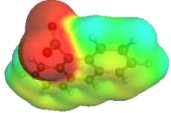
| | | | |
|---|--|--|--|
| <p>TPB</p>  | <p>CCCP</p>  | <p>6-OH-BDE47</p>  | <p>bis(fluorosulfonyl)azide</p>  |
| <p>dino2terb</p>  | <p>dinoseb</p>  | <p>PCP</p>  | <p>bromoxynil</p>  |
| <p>triclosan</p>  | <p>coumachlor</p>  | <p>4-nitro-2-(trifluoromethyl)-1H-benzimidazole</p>  | <p>3,4-Dnp</p>  |
| <p>bromol</p>  | <p>2,4-Dnp</p>  | <p>warfarin</p>  | <p>flufenamate</p>  |
| <p>3,5-Dcp</p>  | <p>4-Np</p>  | <p>diclofenac</p>  | <p>4-octylbenzenesulfonate</p>  |
| <p>sulcotrione</p>  | <p>salicylate</p>  | <p>9,10-dimethoxyanthracene-2-sulfonate salicylate</p>  | <p>anthracene-9-carboxylate</p>  |

Fig. S4 Sigma surfaces (COSMOtherm) of anions measured in this study. Bright red corresponds to high negative surface charge densities, while green corresponds to neutral charge densities. The compounds are ordered after their hexadecane/water partition coefficients (high to low; left to right, up to down). Overall, with decreasing hexadecane/water partition coefficient, the polarity increases.

Table S2 IUPAC Name, Born radius approximated by the van der Waals radius (v.d.W.)^a or by the Einstein-Stokes equation (E.-S.)^b, Calculated (either by the UFZ - LSER database^c or COSMOtherm^d) logarithmic neutral bulk Partition coefficient hexadecane/water $K_{hd/w}$, Calculated logarithmic Anion-Permeability (Monomer) based on stated radii and partition coefficients^c.

| IUPAC Name | r / Å | | Log [$K_{neutral, hd/w} / (L_w/L_{hd})$] | | Log [$(P_{calc} / (cm/s))$] | | |
|--|----------|---------|--|------------|-------------------------------|------------|----------------|
| | | | UFZ - database | COSMOtherm | UFZ - database | COSMOtherm | UFZ - database |
| | v. d. W. | E. – S. | | | v. d. W. | v. d. W. | E. – S. |
| tetraphenylboranuide | 4.2 | 5.8 | | | | | |
| 2-[(3-chlorophenyl)hydrazinylidene]propanedinitrile | 3.4 | 4.7 | 0.7 | -1.0 | -10.1 | -11.8 | -5.0 |
| 3,5-dibromo-2-(2,4-dibromophenoxy)phenol | 3.9 | 7.1 | 1.8 | 4.2 | -6.8 | -4.5 | 0.4 |
| bis(fluorosulfonyl)azanide | 2.9 | 4.4 | | | | | |
| 2-(2-Methyl-2-propanyl)-4,6-dinitrophenol | 3.6 | 5.1 | 2.4 | 3.0 | -7.0 | -6.4 | -2.3 |
| 2-butan-2-yl-4,6-dinitrophenol | 3.6 | 5.1 | 2.1 | 3.1 | -7.4 | -6.3 | -2.7 |
| 2,3,4,5,6-pentachlorophenol | 3.4 | 5.3 | 3.0 | 3.6 | -7.9 | -7.3 | -1.2 |
| 3,5-dibromo-4-hydroxybenzoxonitrile | 3.2 | 5.4 | 0.6 | 1.6 | -11.0 | -10.0 | -3.4 |
| 5-chloro-2-(2,4-dichlorophenoxy)phenol | 3.7 | 5.5 | 2.9 | 3.5 | -6.4 | -5.7 | -0.9 |
| 3-[1-(4-chlorophenyl)-3-oxobutyl]-4-hydroxychromen-2-one | 4.1 | 5.9 | -0.2 | 2.0 | -7.9 | -5.6 | -3.2 |
| 4-nitro-2-(trifluoromethyl)-1H-benzimidazole | 3.3 | 5.0 | -0.4 | -4.8 | -11.3 | -15.7 | -5.4 |
| 3,4-dinitrophenol | 3.0 | 4.5 | -2.6 | -4.3 | -15.4 | -17.1 | -8.8 |
| 2,4,6-tribromophenol | 3.2 | 5.8 | 2.2 | 3.6 | -9.4 | -8.0 | -1.0 |

| | | | | | | | |
|---|-----|-----|-------------------|------|-------|-------|-------|
| 2,4-dinitrophenol | 3.2 | 4.5 | 0.4 | 0.9 | -11.5 | -11.0 | -5.8 |
| 4-hydroxy-3-(3-oxo-1-phenylbutyl)chromen-2-one | 4.0 | 5.7 | -0.1 | 1.7 | -8.0 | -6.2 | -3.6 |
| 2-[3-(trifluoromethyl)anilino]benzoic acid | 3.8 | 5.4 | 2.5 | 2.7 | -6.5 | -6.3 | -1.4 |
| 3,5-dichlorophenol | 3.0 | 4.2 | 0.3 | -0.0 | -12.5 | -12.8 | -6.7 |
| 4-nitrophenol | 3.0 | 3.9 | -2.0 | -3.5 | -15.0 | -16.6 | -10.0 |
| 2-[2-(2,6-dichloroanilino)phenyl]acetate | 3.8 | 5.6 | 1.6 | 1.9 | -7.1 | -6.8 | -2.1 |
| 4-octylbenzenesulfonate | 4.0 | 5.3 | 2.1 ^f | 1.1 | -6.0 | -7.0 | -2.0 |
| 2-(2-chloro-4-methylsulfonylbenzoyl)cyclohexane-1,3-dione | 4.0 | 5.8 | -1.4 ^f | -2.1 | -9.6 | -10.3 | -4.6 |
| 2-hydroxybenzoic acid | 3.0 | 3.9 | -0.7 | -1.0 | -13.4 | -13.8 | -8.8 |
| 9,10-dimethoxyanthracene-2-sulfonate | 4.0 | 5.7 | -0.3 ^f | -1.1 | -8.4 | -9.2 | -3.6 |
| anthracene-9-carboxylic acid | 3.6 | 4.9 | 1.4 | 0.5 | -8.2 | -9.2 | -3.8 |

^a Van der Waals volume was predicted using JChem for Office (Excel), JChem for Office 17.14.0.1746, 2017 ChemAxon (<http://www.chemaxon.com>), and r calculated under the assumption of a perfect sphere. ^b Einstein-Stokes equation: $D_{aq} = k_b T / (6\pi\eta r)$, where D_{aq} is the diffusion constant in water (see Table S1, $D_{aq} = 10^{-5.13-0.453 \cdot \log(MW)}$), k_b is Boltzmann's constant, r is the radius of the spherical particle, η is the dynamic viscosity of water ($0.69 \cdot 10^{-3} \text{ N} \cdot \text{s} / \text{m}^2 @ 25^\circ \text{C}$ (6)). ^c Ref. (7). ^d COSMOtherm (8), C30_18, COSMOlogic GmbH & Co KG, <http://www.cosmologic.de>. ^e Image energy was calculated according to Eq. 8 for the effective bilayer thickness of 25.5 Å, dipole energy was calculated for the dipole potential of 228 mV according to Eq. 6, and Born energy was calculated according to Eq. 7 using either the van der Waals radius or the radius predicted by the Einstein-Stokes equation. The predicted neutral hexadecane/water partition coefficients (UFZ-LSER database / COSMOtherm) were corrected for image, dipole and Born energy in the membrane, and the permeability was then calculated using Eq. 2. ^f Calculated descriptors used for UFZ-LSERD calculation, experimental descriptors for all other compounds.

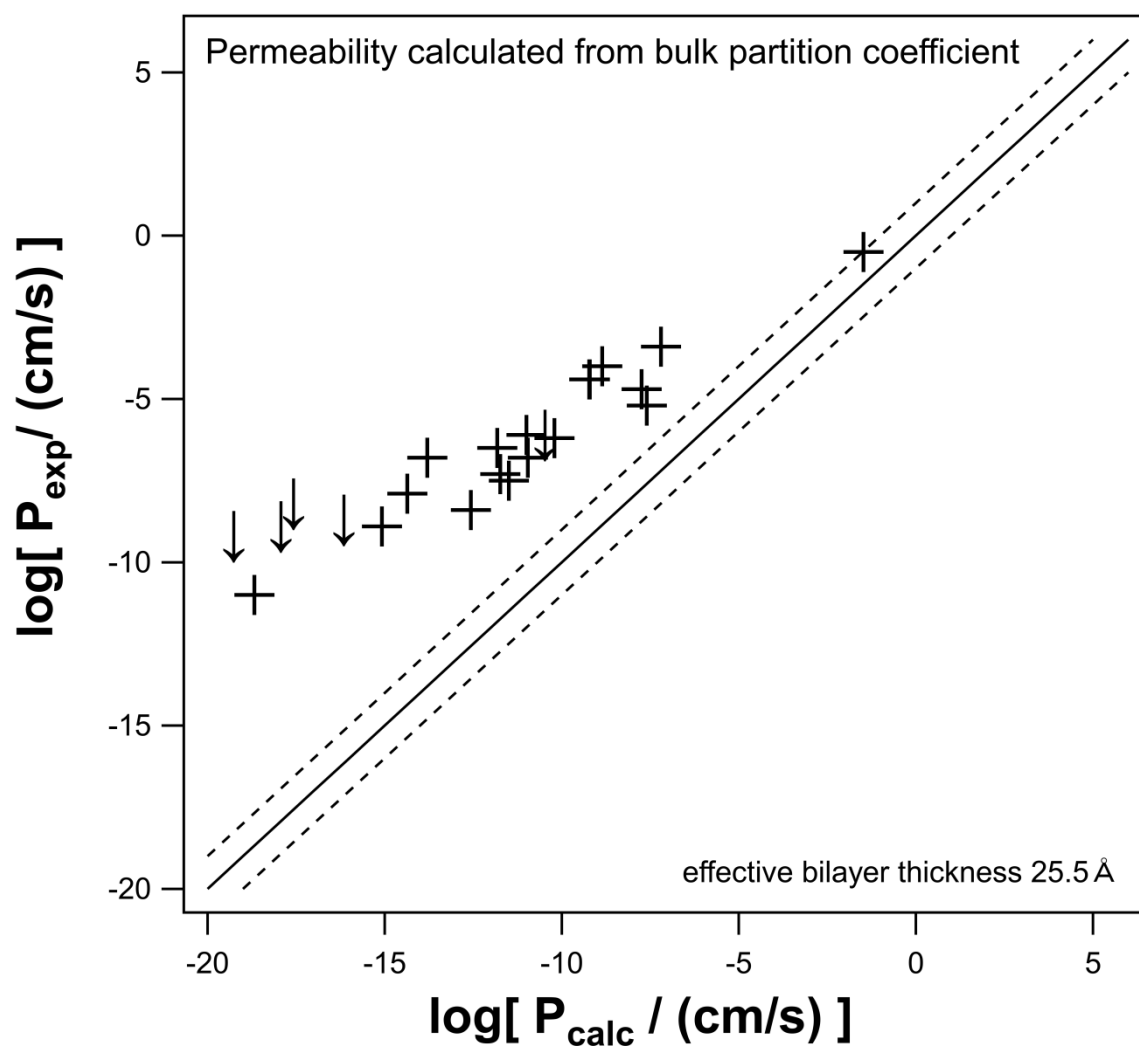


Fig. S5 Experimental permeability plotted against the permeability calculated based on the bulk hexadecane/water partition coefficient of the anion predicted with COSMOtherm. The predicted bulk partition coefficient (COSMOtherm) was corrected for dipole and image energy inside the membrane, and the permeability was calculated using Eq. 2, for the effective bilayer thickness of $d = 25.5 \text{ \AA}$. The solid line shows the identity line (1:1); deviations of ± 1 log unit are indicated as dashed lines. The slower and more polar the ions, the bigger the deviation from the identity line.

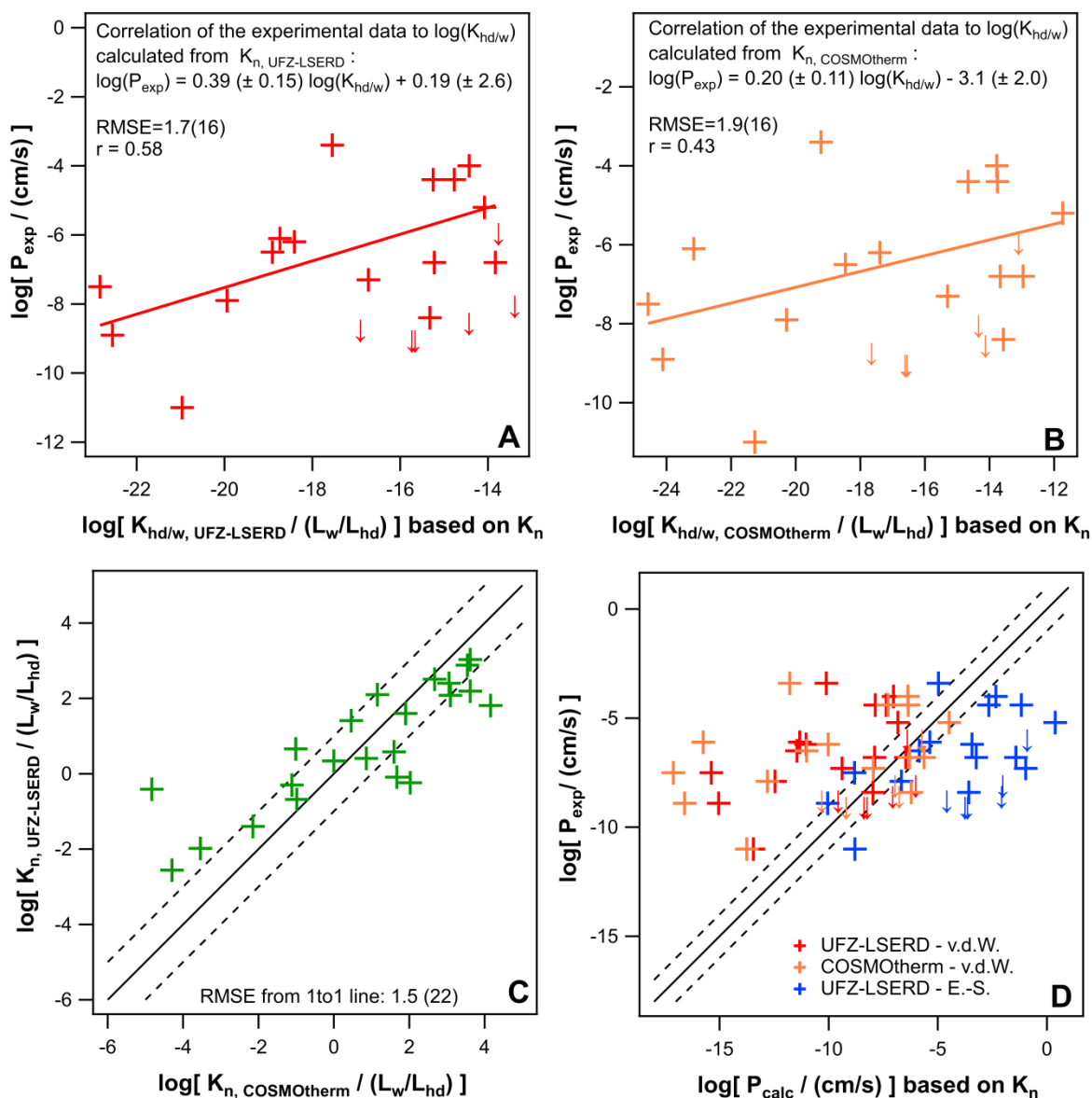


Fig. S6 Experimental permeability data plotted against the calculated bulk anionic partition coefficients $K_{hd/w}$ based on the neutral partition coefficients K_n calculated by the UFZ-LSER database (A) or predicted by COSMOtherm (B). Downward arrows indicate upper limits of the experimental permeability. Both plots show broadly distributed datapoints with an RMSE of 1.7 and 1.9 respectively. In (C) the neutral partition coefficients calculated by the UFZ-LSER database $K_{n, UFZ-LSERD}$ and by COSMOtherm $K_{n, COSMOtherm}$ are plotted against each other. The solid line shows the identity line (1:1); deviations of ± 1 log unit are indicated as dashed lines. The RMSE from the identity line is 1.5. Errors in K_n cannot explain the scatter in (A) and (B). Instead, errors in the Born radius can lead to errors of several orders of magnitude in the calculated permeability. In (D), the experimental permeability is plotted against the calculated anion permeability, once for calculations based on a Born radius estimated from the van der Waals radius (red, orange), or calculated by the Einstein - Stokes equation (blue). While the calculations based on $K_{n, UFZ-LSERD}$ or $K_{n, COSMOtherm}$ using the van der Waals radius do not differ by much, the calculated permeability is increased by several orders of magnitude using the Einstein - Stokes radius. Plotted data are listed in Table S2 and Table 1.

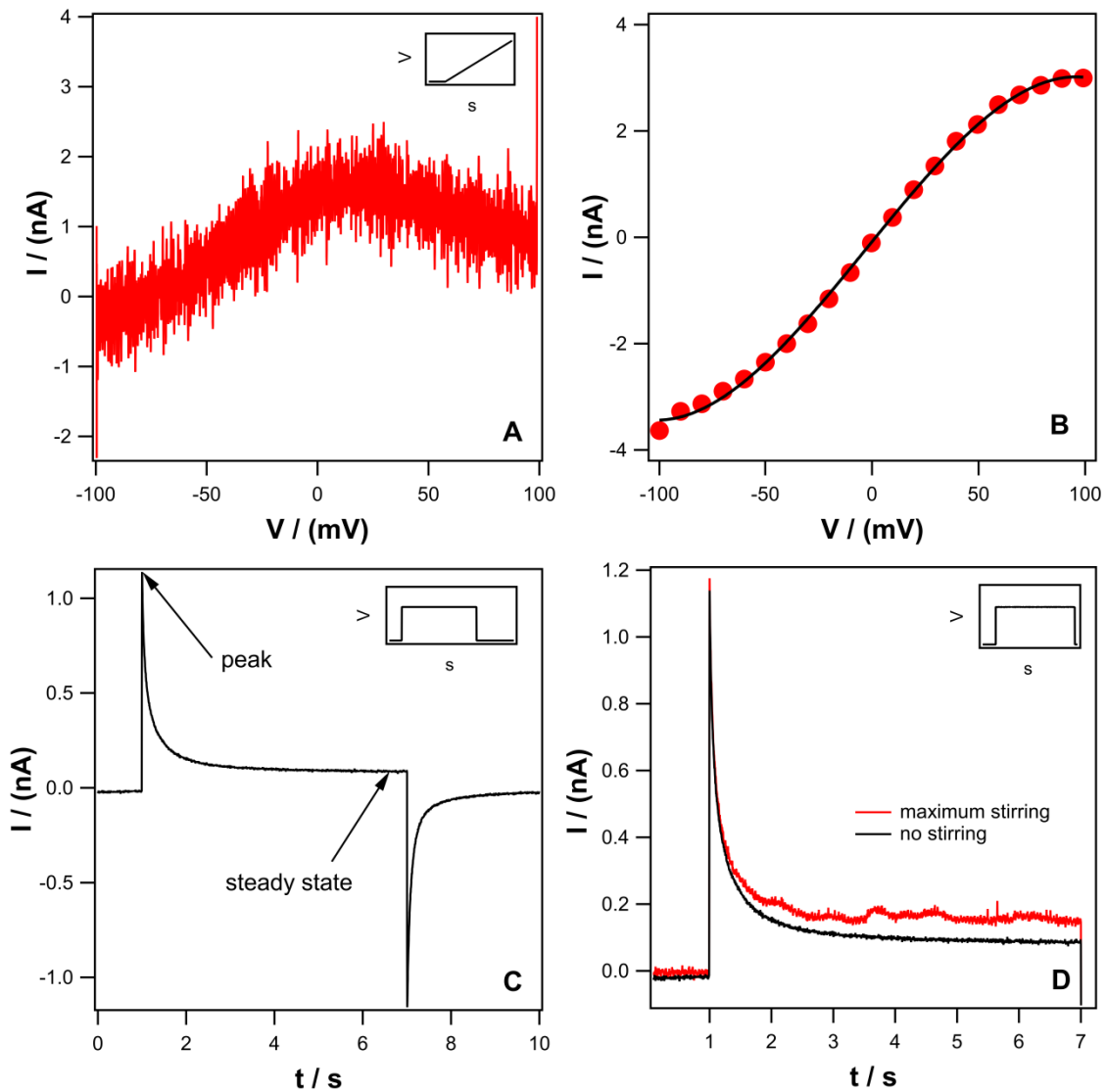


Fig. S7 Characteristic curves of TPB. (A) Negative I/V characteristic (TPB; 60nM): Although the applied voltage ramp increases continuously, the current decreases for higher positive voltages. This effect is explained by a superposition of the not yet reached steady state currents and the decaying initial current peak (TPB; 7.8 μ M) after voltage application (C). Steady state I/V curves limited by diffusion polarization show no superlinearity, but saturate with increasing voltage (TPB; 220nM) (B). Only in permeation processes limited by the diffusion through the UWL, effects due to stirring could be detected. At maximum stirring, the steady state current is higher and is reached faster than without stirring (TPB; 7.8 μ M) (D).

Table S3 Saturation behavior of anions measured in this study^a: Compound name, Abbreviation, logarithmic concentration $\log(K_m)$ at which half of the saturating conductivity is reached, and logarithmic permeability $\log(P)$.

| Compound name | Abbreviation | Log [K_m / M] | Log [(P / (cm/s))] |
|---|--------------|-------------------|-----------------------|
| Tetraphenylboranuide | TPB | -6.8 | -0.5 |
| 2-[(3-chlorophenyl)hydrazinylidene]propanedinitrile | CCCP | -4.7 | -3.4 |
| bis(fluorosulfonyl)amide | | -3.8 | -4.7 |
| 2-(2-Methyl-2-propanyl)-4,6-dinitrophenol | dino2terb | -5 | -4.0 |
| 2-butan-2-yl-4,6-dinitrophenol | dinoseb | -4.7 | -4.4 |
| 2,3,4,5,6-pentachlorophenol | PCP | -5.31 | -4.4 |
| 3,5-dibromo-4-hydroxybenzonitrile | bromoxynil | -3.1 | -6.2 |

^a For all anions that showed saturating conductivity the concentration K_m at which half of the saturating current was reached was extracted using Eq. 11.

Table S4 Saturation behavior of anions from literature^a: Compound name, Abbreviation, logarithmic concentration $\log(K_m)$ at which half of the saturating conductivity is reached, and logarithmic permeability $\log(P)$.

| Compound name | Abbreviation | Log [K_m / M] | Log [(P/(cm/s)) |
|---|-----------------------------|-------------------|-------------------|
| 2,4,6-trinitro-N-(2,4,6-trinitrophenyl)aniline | DPA ^b | -7.4 | 0.9 |
| 3-tert-butyl-5-chloro-N-(2-chloro-4-nitrophenyl)- 2-hydroxybenzamide | S13 ^c | -6.6 | 0.8 |
| 2-[[4-(trifluoromethoxy) phenyl]hydrazinylidene]propanedinitrile | FCCP ^d | -5.9 | 0.3 |
| 2-hydroxybenzoic acid | salicylic acid ^e | -2.4 | -7.1 |

^a For all anions from literature that showed saturating conductivity, conductivity values were extracted from conductivity/concentration plots, and the concentration K_m at which half of the saturating current was reached was extracted using Eq. 11. Permeabilities were determined as listed in Table S7. ^b Conductivity at 25°C extracted from Fig. 7 in Ref. (1), in DOPC/decane. ^c Conductivity at 22°C extracted from Fig. 6 in Ref. (9), in DPhPC/chlorodecane. ^d Conductivity at 22°C extracted from Fig. 7 in Ref. (10), in PE/chlorodecane. ^e Conductivity at 22°C extracted from Fig. 3 in Ref. (11), in DPhPC/chlorodecane/decane (50%, vol/vol).

Table S5 Saturation behavior of cations from literature^a: Compound name, Abbreviation, logarithmic concentration $\log(K_m)$ at which half of the saturating conductivity is reached, and logarithmic permeability $\log(P)$.

| Compound name | Abbreviation | Log [K_m / M] | Log [(P / (cm/s))] |
|----------------------------|--------------|-------------------|-----------------------|
| tetraphenylphosphonium | TPP | -4.6 | -5.2 |
| triphenylmethylphosphonium | TPMP | -3.4 | -7.5 |
| triphenylethylphosphonium | TPEP | -3.7 | -6.3 |
| triphenylpropylphosphonium | TPPP | -3.3 | -6.1 |
| triphenylbutylphosphonium | TPBP | -3.3 | -5.9 |
| triphenylamylphosphonium | TPAP | -4.7 | -4.9 |
| triphenylhexylphosphonium | TPHP | -4.9 | -4.6 |

^a All cationic saturation data (measured in solvent free bilayers, PC from asolectin) were taken from Table I in Ref. (12). K_m were taken as stated, the permeability was calculated for infinite dilution (combining Eq. 10 and 11) using $P=R*T/(z*F)^2*(G_{s,0,max}/K_m)$.

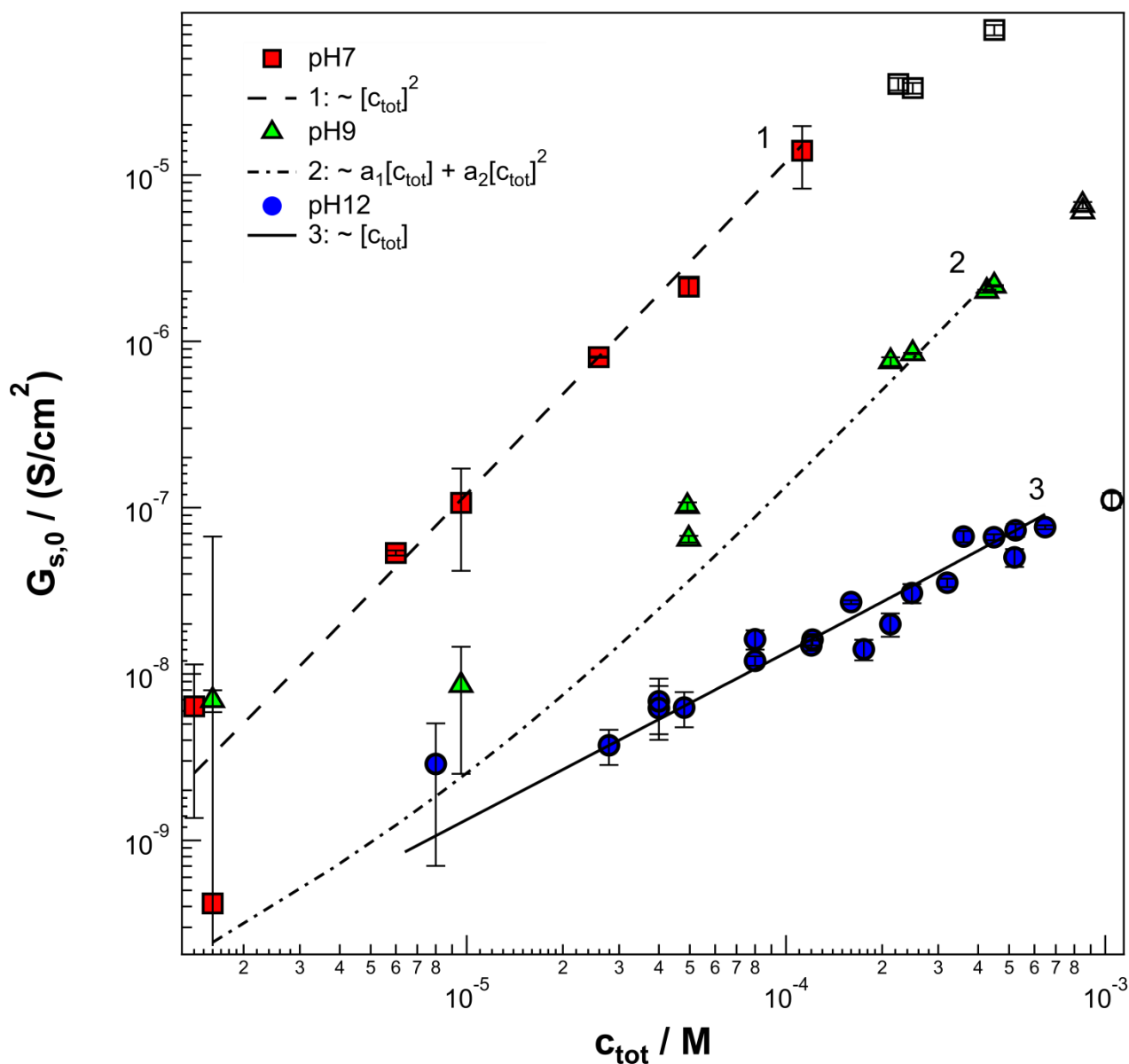


Fig. S8 Conductivity of 3,4-Dnp measured at three different pH (pH7 red squares, pH9 green triangles, and pH12 blue circles) plotted against the total concentration $c_{\text{tot}} = c_{\text{anion}} + c_{\text{neutral}} + 2c_{\text{heterodimer}}$. The dashed line (1) is directly proportional to the square of c_{tot} , indicating that at pH7 heterodimer permeation dominates, while the solid line (3) is directly proportional to c_{tot} , indicating that at pH12 monomeric permeation dominates, as with increasing pH c_{anion} increases and $c_{\text{heterodimer}}$ decreases (see Eq. S3 and S5). The dot-dashed line (2) shows linear dependencies at low concentrations, but quadratic dependencies for higher concentrations. In the transition, neither heterodimer nor monomer permeation dominate, but both processes run in parallel and sum up to the final measured conductivity (see Fig. S3).

Table S6 Experimental Anion-Permeability, logarithmic Experimental Anion-Permeability, and the Deviation factor between different lipids and DPhPC for the compounds coumachlor and dino2terb. Both chemicals were measured in four different lipid compositions: DOPC, DPHPC, DPhPC+20mol% cholesterol, and PLE. None of the measurements in different lipids deviated by more than a factor of 0.3 or 2.6 from measurements in DPhPC.

| Chemical | Membrane | Deviation factor | | |
|------------|-------------------|----------------------------------|---|---|
| compound | lipid composition | $P_{\text{exp}} / (\text{cm/s})$ | $\text{Log} [P_{\text{exp}} / (\text{cm/s})]$ | $P_{\text{exp}} (\text{lipid}) / P_{\text{exp}} (\text{DPhPC})$ |
| coumachlor | DOPC | $4.4 \cdot 10^{-7}$ | -6.3 | 2.6 |
| | DPhPC | $1.7 \cdot 10^{-7}$ | -6.8 | 1 |
| | DPhPC+20mol% | $9.6 \cdot 10^{-8}$ | -7.0 | 0.6 |
| | cholesterol | | | |
| | PLE | $7.2 \cdot 10^{-8}$ | -7.1 | 0.4 |
| dino2terb | DOPC | $1.8 \cdot 10^{-4}$ | -3.7 | 1.6 |
| | DPhPC | $1.1 \cdot 10^{-4}$ | -3.9 | 1 |
| | DPhPC+20mol% | $1.0 \cdot 10^{-4}$ | -4.0 | 0.9 |
| | cholesterol | | | |
| | PLE | $3.2 \cdot 10^{-5}$ | -4.5 | 0.3 |

Table S7 IUPAC Name, Abbreviation, Experimental logarithmic Anion-Permeability (Monomer, from **literature**) through the listed bilayer, measured at listed pH, pK_a (experimental/predicted), Calculated logarithmic anionic bulk Partition coefficient chlorodecane/water $K_{cd/w}$, and hexadecane/water $K_{hd/w}$.

| IUPAC Name | Abbreviation | Log [P _{lit} / (cm/s)] | bilayer | pH | pK _a | Log [K _{cd/w} / (L _w /L _{cd})] | Log [K _{hd/w} / (L _w /L _{hd})] |
|---|--------------|-----------------------------------|--|-----|-------------------|---|---|
| 3-tert-butyl-5-chloro-N-(2-chloro-4-nitrophenyl)-2-hydroxybenzamide | S13 | 0.8 ^a | DPhPC / chlorodecane | 8.3 | 5.8 ^b | -9.0 | -14.7 |
| 2-[[4-(trifluoromethoxy)phenyl]hydrazinylidene]propanedinitrile | FCCP | 0.3 ^c | PE / chlorodecane | 8.4 | 6.05 ^d | -8.1 | -13.4 |
| 2-[[4-(trifluoromethoxy)phenyl]hydrazinylidene]propanedinitrile | FCCP | -4.2 ^e | bull brain extract / heptane | 7.5 | 6.05 ^d | | -13.4 |
| 2-[(3-chlorophenyl)hydrazinylidene]propanedinitrile | CCCP | -0.5 ^f | DPhPC / chlorodecane | 8.3 | 6.09 ^g | -9.0 | -14.6 |
| 2-[(3-chlorophenyl)hydrazinylidene]propanedinitrile | CCCP | -2.7 ^h | PC / cholesterol (50/50) / decane ⁱ | 7 | 6.09 ^g | | -14.6 |
| 2-[(3-chlorophenyl)hydrazinylidene]propanedinitrile | CCCP | -4.9 ^e | bull brain extract / heptane | 7.5 | 6.09 ^g | | -14.6 |
| 2,4,6-trinitrophenol | TNP | -6.5 ^e | bull brain extract / heptane | 7.5 | 2.0 ^j | | -15.7 |
| 2,4-dinitrophenol | 2,4-Dnp | -7.8 ^e | bull brain extract / heptane | 7.5 | 4.3 ^j | | -19.2 |
| 2,3,4,5,6-pentachlorophenol | PCP | -6.1 ^e | bull brain extract / heptane | 7.5 | 4.8 ^l | | -16.6 |

| | | | | | | | |
|--|----------------|--------------------|---|-----|-------------------|-------|-------|
| 2,3,4,5,6-pentachlorophenol | PCP | -3.5 ^k | PC / cholesterol(20/80) /decane | 7 | 4.8 ^l | | -16.6 |
| cyano(triphenyl)boranuide | TPCB | -2.8 ^m | DOPC / decane ⁿ | | - | | -12.8 |
| tetrakis(4-chlorophenyl) boranuide | TCPB | 1.9 ^m | DOPC / decane | | - | | -1.8 |
| tetrakis(3-trifluoromethylphenyl) boranuide | TTFPB | 2.2 ^m | DOPC / decane | | - | | 1.1 |
| tetrakis(4-fluorophenyl)boranuide | TFPB | 1.4 ^m | DOPC / decane | | - | | -4.5 |
| tetraethylboranuide | TEB | >-1.0 ^m | DOPC / decane | | - | | -11.4 |
| tetraphenylboranuide | TPB | -0.8 ^m | DOPC / decane | | - | | -8.8 |
| tetraphenylboranuide | TPB | -0.6 ^o | DOPC / decane | 6 | - | | -8.8 |
| 2,4,6-trinitro-N-(2,4,6- trinitrophenyl)aniline | DPA | 0.9 ^o | DOPC / decane | 6 | -1.8 ^j | | -8.0 |
| thiocyanate | CNS | -7.8 ^p | DPhPC / solvent depleted | 7.5 | 0.5 ^j | | -22.5 |
| thiocyanate | CNS | -5.8 ^p | DPhPC / chlorodecane | 7.5 | 0.5 ^j | -16.4 | -22.5 |
| perchlorate | | -8.7 ^p | DPhPC / solvent depleted | 7.5 | -7.1 ^j | | -22.3 |
| perchlorate | | -5.8 ^p | DPhPC / chlorodecane | 7.5 | -7.1 ^j | 16.2 | -22.3 |
| 2-hydroxybenzoic acid | salicylic acid | -7.1 ^q | DPhPC / chlorodecane / decane (50%, vol/vol) | 7.8 | 2.8 ^j | -18.3 | -26.1 |
| benzoic acid | benzoic | -8.8 ^r | DPhPC / chlorodecane / decane (50%, vol/vol) | 7.8 | 4.1 ^j | -23.8 | -30.7 |

| | | | | | | | |
|---|---------|--------------------|---|-----|------------------|-------|-------|
| 2-acetyloxybenzoic acid | aspirin | -8.9 ^r | DPhPC / chlorodecane / decane (50%, vol/vol) | 7.8 | 3.4 ⁱ | -23.6 | -30.6 |
| 3-hydroxybenzoic acid | | <-9.9 ^f | DPhPC / chlorodecane / decane (50%, vol/vol) | 7.8 | 3.8 ⁱ | -26.6 | -33.6 |
| 2,6-dihydroxybenzoic acid | | -6.2 ^r | DPhPC / chlorodecane / decane (50%, vol/vol) | 7.8 | 1.6 ^j | -16.4 | -22.3 |
| 5,6-dichloro-2-(trifluoromethyl)-1H- benzimidazole | DTFB | -1.5 ^s | PC / chlorodecane | 9.3 | 7.3 ^t | -10.0 | -15.6 |

^a Permeability at 22°C extracted from Fig. 6 in Ref. (9). ^b From Ref. (9). ^c Permeability at 22°C extracted from Fig. 7 in Ref. (10). ^d From Ref. (10). ^e Permeability at room temperature extracted from Table I in Ref. (13). ^f Permeability at 22°C extracted from Fig. 5 in Ref. (14). ^g From Ref. (15). ^h Permeability at 26°C, Ref. (15). ⁱ According to the LeBlanc (15), this lipid composition leads to one order of magnitude or more higher background conductance. ^j JChem for Office (Excel) was used for pK_a calculation, JChem for Office 17.14.0.1746, 2017 ChemAxon (<http://www.chemaxon.com>). ^k Permeability at 22-23°C extracted from Fig. 2 in Ref. (16), value at 25mV. ^l From Ref. (16). ^m Permeability/(β*k_i) at 25°C extracted from Table II in Ref. (17). ⁿ DEPC/decane membranes led to about 10 times higher permeabilities, see Ref. (17). ^o Permeability/conductivity at 25°C extracted from Table 1 in Ref. (1). ^p Permeability at 20-22°C extracted from Fig. 2 in Ref. (18). ^q Permeability at 22°C extracted from Fig. 3 in Ref. (11). ^r Permeability/conductivity at 22°C extracted from Table in Ref. (11). ^s Permeability at 22-23°C extracted from Fig. 8 in Ref. (19). ^t From Ref. (19).

SUPPORTING REFERENCES

1. Ketterer, B., B. Neumcke, and P. Läuger. 1971. Transport mechanism of hydrophobic anions through lipid bilayer membranes. *J Membr. Biol.* 5: 225–245.
2. Borisova, M.P., L.N. Ermishkin, E.A. Liberman, A.Y. Silberstein, and E.M. Trofimov. 1974. Mechanism of conductivity of bimolecular lipid membranes in the presence of tetrachlorotrifluoromethylbenzimidazole. *J. Membr. Biol.* 18: 243–261.
3. Pohl, P., S.M. Saporov, and Y.N. Antonenko. 1998. The size of the unstirred layer as a function of the solute diffusion coefficient. *Biophys. J.* 75: 1403–1409.
4. Avdeef, A. 2010. Leakiness and Size Exclusion of Paracellular Channels in Cultured Epithelial Cell Monolayers—Interlaboratory Comparison. *Pharm. Res.* 27: 480–489.
5. Bittermann, K., and K.U. Goss. 2017. Assessing the toxicity of ionic liquids – Application of the critical membrane concentration approach. *Chemosphere.* 183: 410–418.
6. Crittenden, J.C., R.R. Trussell, D.W. Hand, K.J. Howe, and G. Tchobanoglous. 2012. *MWH's Water Treatment: Principles and Design: Third Edition.* MWH's Water Treat. Princ. Des. Third Ed. .
7. Ulrich S.; Brown, T.N.; Watanabe, N.; Bronner, G.; Abraham, M.H.; Goss, K.-U., N.. E. 2017. UFZ-LSER database v 3.2 [Internet]. .
8. Eckert, F., and A. Klamt. 2002. Fast solvent screening via quantum chemistry: COSMO-RS approach. *AIChE J.* 48: 369–385.
9. Kasianowicz, J., R. Benz, and S. McLaughlin. 1987. How Do Protons Cross the Membrane-Solution Interface - Kinetic-Studies on Bilayer-Membranes Exposed To the Protonophore-S-13 (5-Chloro-3-Tert-Butyl-2'-Chloro-4'- Nitrosalicylanilide). *J. Membr. Biol.* 95: 73–89.
10. Benz, R., and S. McLaughlin. 1983. The molecular mechanism of action of the proton ionophore FCCP (carbonylcyanide p-trifluoromethoxyphenylhydrazone). *Biophys. J.* 41: 381–398.
11. Gutknecht, J. 1990. Salicylates and proton transport through lipid bilayer membranes: A model for salicylate-induced uncoupling and swelling in mitochondria. *J. Membr. Biol.* 115: 253–260.
12. Miyauchi, S., A. Ono, M. Yoshimoto, and N. Kamo. 1993. Membrane transport of tetraphenylphosphonium and its homologues through the planar phospholipid bilayer: Concentration dependence and mutually competitive inhibition in membrane passive transport. *J. Pharm. Sci.* 82: 27–31.
13. Liberman, E.A., and V.P. Topaly. 1968. Selective transport of ions through bimolecular phospholipid membranes. *BBA - Biomembr.* 163: 125–136.
14. Kasianowicz, J., R. Benz, and S. McLaughlin. 1984. The kinetic mechanism by which CCCP (carbonyl cyanide m-Chlorophenylhydrazone) transports protons across membranes. *J. Membr. Biol.* 82: 179–190.
15. LeBlanc, O.H. 1971. The effect of uncouplers of oxidative phosphorylation on lipid bilayer membranes: Carbonylcyanide m-chlorophenylhydrazone. *J. Membr. Biol.* 4: 227–251.
16. Smejtek, P., K. Hsu, and W.H. Perman. 1976. Electrical conductivity in lipid bilayer membranes induced by pentachlorophenol. *Biophys. J.* 16: 319–336.
17. Benz, R. 1988. Structural requirement for the rapid movement of charged molecules across membranes. Experiments with tetraphenylborate analogues. *Biophys. J.* 54: 25–33.
18. Dilger, J.P., S.G. McLaughlin, T.J. McIntosh, and S.A. Simon. 1979. The dielectric constant of phospholipid bilayers and the permeability of membranes to ions. *Science.* 206: 1196–1198.

19. Dilger, J., and S. McLaughlin. 1979. Proton transport through membranes induced by weak acids: A study of two substituted benzimidazoles. *J. Membr. Biol.* 46: 359–384.